

FAST MAGNETIC FIELD AMPLIFICATION IN THE EARLY UNIVERSE: GROWTH OF COLLISIONLESS PLASMA INSTABILITIES IN TURBULENT MEDIA

D. FALCETA-GONÇALVES^{1,2} & G. KOWAL²*Draft version December 20, 2021*

ABSTRACT

In this work we report a numerical study of the cosmic magnetic field amplification due to collisionless plasma instabilities. The collisionless magnetohydrodynamic equations derived account for the pressure anisotropy that leads, in specific conditions, to the firehose and mirror instabilities. We study the time evolution of seed fields in turbulence under the influence of such instabilities. An approximate analytical time evolution of magnetic field is provided. The numerical simulations and the analytical predictions are compared. We found that i) amplification of magnetic field was efficient in firehose unstable turbulent regimes, but not in the mirror unstable models, ii) the growth rate of the magnetic energy density is much faster than the turbulent dynamo, iii) the efficient amplification occurs at small scales. The analytical prediction for the correlation between the growth timescales with pressure anisotropy ratio is confirmed by the numerical simulations. These results reinforce the idea that pressure anisotropies - driven naturally in a turbulent collisionless medium, e.g. the intergalactic medium -, could efficiently amplify the magnetic field in the early Universe (post-recombination era), previous to the collapse of the first large-scale gravitational structures. This mechanism, though fast for the small scale fields (\sim kpc scales), is however unable to provide relatively strong magnetic fields at large scales. Other mechanisms that were not accounted here (e.g., collisional turbulence once instabilities are quenched, velocity shear, or gravitationally induced inflows of gas into galaxies and clusters) could operate afterwards to build up large scale coherent field structures in the long time evolution.

Subject headings: intergalactic medium — magnetic fields — turbulence — MHD

1. INTRODUCTION

The baryonic fraction of the intergalactic medium (IGM) is composed by dilute warm/hot plasmas. Depending on the local environment the plasma properties of the IGM may be different. For instance, the most diffuse component of the IGM, known as intergalactic “voids”, are vast regions between clusters of galaxies in the Universe as seen today. Filaments of somewhat compressed and warmer ($10^5 - 10^7$ K) gas form what is broadly understood as the IGM, while the denser ($\sim 10^{-3}\text{cm}^{-3}$) and shock heated ($\sim 10^7 - 10^8$ K) plasma in clusters of galaxies are known as the intracluster medium (ICM). For many decades the intracluster medium is known to be magnetized (see reviews by Kronberg 1994; Enßlin et al. 2005; Widrow et al. 2012; Durrer & Neronov 2013, and references therein), but unfortunately any constraints on the magnetization of the IGM and intergalactic voids lack of more substantial observational confirmation. The magnetic intensity and its respective correlation length must naturally be related to the processes from which they originate and/or amplify, which depend on local dynamical and physical properties. However, the origin and/or amplification of the magnetic fields at cosmological scales are not completely understood yet, and represent a long standing major issue in modern astrophysics.

Seed fields may have been generated at the pre-equipartition epoch by subatomic scale processes, such as

hadron phase transitions, or at later (post-equipartition) and pre-galactic epoch by large-scale magnetohydrodynamical (MHD) processes, e.g. the $\nabla p \times \nabla \rho$ battery term from Ohm’s Law (Biermann 1950), currents induced by electronic scattering of anisotropic radiation fields (Langer et al. 2005; Durrive & Langer 2014), evolution of turbulent fields (e.g. Banerjee & Jedamzik 2004, and many others), and even shock excited Weibel instabilities (Schlickeiser & Shukla 2003; Schlickeiser 2005). (Jedamzik et al. 1998) suggests however that photon diffusion damping would affect post-equipartition, but pre-recombination, magnetic fluctuations. Therefore most of the amplification processes mentioned above would only be important after recombination era. These could in principle generate magnetic fields with intensities of the order of $10^{-30} - 10^{-11}$ G. There are several implications of a strong magnetic field on the cosmological evolution of the Universe, from primordial nucleosynthesis to the statistics of the cosmic microwave background (CMB). Current data limits the primordial (comoving) magnetic field intensity to $B_{1\text{Mpc}} < 5\text{nG}$ at 1Mpc lengthscale (see Trivedi et al. 2010; Planck Collab. 2014, for references on WMAP and PLANCK data analysis, respectively). Such field intensities are below the values inferred for the ICM ($B \sim 0.1 - 10 \mu\text{G}$ (see Govoni & Feretti 2004, and references therein)), as well as for more diffuse groups of galaxies (e.g. Nikiel-Wroczyński et al. 2013). Recently, arguable lower limits for the magnetization of the diffuse intergalactic medium have been also provided based on gamma-ray observations of blazars (see Neronov & Vovk 2010). These evidences combined together suggest that the Universe was magnetized even before the structure formation. Therefore, the problem seems to be twofold:

¹ SUPA, School of Physics & Astronomy, University of St Andrews, North Haugh, St Andrews, Fife KY16 9SS, UK

² Escola de Artes, Ciências e Humanidades, Universidade de São Paulo, Rua Arlindo Bettio, 1000, São Paulo, SP 03828-000, Brazil

the first being the actual origin of the magnetic fields (seed fields), which may have occurred very early in the Universe history (pre-equipartition); and the second being the amplification of such seed fields to the values observed in the diffuse gas of clusters of galaxies.

Observations of the Faraday rotation (FR) effect provide currently the best estimates for the IGM magnetic fields. In the FR effect the position angle of linearly polarized radiation shifts on the plane of sky as a function of wavelength λ as $\Delta\phi = RM \times \lambda^2$, with the rotation measure RM being $RM(\text{rad/m}^2) \simeq 812 \int_0^{L(\text{kpc})} n_e(\text{cm}^{-3}) B_{\parallel}(\mu\text{G}) dl$, where \parallel denotes the direction parallel to the line of sight.

It is well-known that RM strongly depends on the spatial distribution of the electron density (n_e) and the magnetic field geometry along the line of sight (B_{\parallel}), and basic geometrical assumptions with respect to them are usually made. It is also natural to presume that the IGM magnetic field is not uniform. Faraday rotation maps present ordered magnetic fluctuations at scales from $\sim 1\text{kpc}$ associated with cooling flows up to $\sim 1\text{Mpc}$ associated to powerful active galactic nuclei (AGN) jets and cluster radio relics (e.g. Ferreti et al. 2012). These lengthscales, however, cannot be directly understood as correlation scales for the magnetic field. Observational estimates of typical lengthscales usually assume an *ad hoc* correlation between the magnetic field and local plasma density in the range of $1 - 30\text{kpc}$ (e.g. Bonafede et al. 2010; Vacca et al. 2012). Unfortunately, given the turbulent nature of the IGM, the actual correlation length (l_{corr}) of the IGM/ICM magnetic field depends also on the spatial distribution of the velocity field (e.g. Burkhart et al. 2009; Xu et al. 2009; Falceta-Gonçalves et al. 2014), and l_{corr} for the magnetic field of the IGM cannot be observationally estimated yet. Still, even though around equipartition level with the thermal and kinetic counterparts, the presence of strong magnetic fields ($B \gtrsim \mu\text{G}$) is surprising, given the general understanding that μG scale fields would be the result of galactic dynamo amplification of much less intense pre-galactic seed fields and the related timescales.

During the last decade several authors have employed numerical simulations and analytical approximate solutions of collisional plasmas to study the magnetic amplification due to turbulent dynamo, galactic fields diffused into the ICM by outflows, and AGNs (see e.g. Dolag et al. 2002; Dubois et al. 2009; Donnert et al. 2009; Falceta-Gonçalves et al. 2010; Xu et al. 2012; Schober et al. 2012, 2013; Cho 2014; Federrath et al. 2014, and references therein). It was found that all these processes could in principle account for the amplification of a pre-existing seed field to observable values. Such degeneracy among different mechanisms could be removed if the correlation lengths of density, velocity and magnetic fields were directly and independently obtained observationally. This because the different processes suggested so far operate at either different scales, or with different cross-correlations between the physical parameters ($\mathbf{B}, n, p, \mathbf{v}$). However, the possibility that μG magnetic fields could be present in vast volumes of the more diffuse intergalactic medium, where the density of galaxies and the impact of AGNs are relatively small, points to the turbulent dynamo as a viable and ubiquitous process.

Great effort on the understanding of turbulent dynamos has been employed by means of analytical and numerical studies (see Schekochihin et al. 2007; Brandenburg et al. 2012; Schober et al. 2012; de Gouveia Dal Pino et al. 2013, and references therein). The turbulent dynamo is the process by which kinetic energy of turbulent motions is converted into magnetic energy. Turbulent cells stretch and fold field lines in a weakly magnetized plasma increasing the total magnetic energy. Such a dynamo can in principle operate at the large range of scales where there is turbulence, depending on the properties of the flow. This was first pointed out by Batchelor (1950), and further developed into the Kraichnan-Kazantsev theory (Kazantsev 1967; Kraichnan 1968). Here, and throughout this paper, we assume the intergalactic plasma to be a highly conducting medium in the sense that the resistivity (η) is much smaller than the viscosity (ν), i.e. the Prandtl number $Pm \equiv \nu/\eta \gg 1$. In this case, the small-scale dynamo (SSD) theory predicts an exponential growth of magnetic energy, up to equipartition at the viscous scale. The power spectrum of the magnetic fluctuations is then proportional to $k^{3/2}$, resulting in a concentration of energy at small scales. Once saturated at small scales, the dynamo enters in a nonlinear phase showing slower amplification rates (linear with time). The scale at which turbulence is dissipated regulates the efficiency of nonlinear phase for the dynamo process. If we consider the standard collisionality of the ICM, the non-linear phase of the turbulent dynamo is possibly of little interest for cosmological magnetic field studies. It has been suggested though that the enhanced effective collisionality due to plasma instabilities could even completely suppress the kinetic phase, and the nonlinear dynamo would be all that is left (see Mogavero & Schekochihin 2014). As we discuss below, for the purpose of this work, the exact determination of the transition between kinetic³ and nonlinear regimes is not relevant. Due to the little understanding of the anomalous collisionality in diffuse media, and the fact that the nonlinear regime is even slower than the kinetic one, we will concentrate only on the early kinetic phase.

We may consider that during the kinetic phase the magnetic field intensity increases as $B(t) = B_0 \exp(t/\tau_d)$, being the timescale $\tau_d = l_d/\delta v_{l_d}$, with δv_{l_d} the turbulent amplitude at the viscous scale l_d . The saturation occurs when $B(t_{\text{sat}}) \simeq \delta v_{l_d} (4\pi\rho)^{1/2} \simeq \delta v_L Re^{-1/4} (4\pi\rho)^{1/2}$, which results in⁴:

$$t_{\text{sat}} \sim 2 \frac{L}{\delta v_L} Re^{-1/2} \ln \left(\mathcal{M}_{A,L}^0 Re^{-1/4} \right), \quad (1)$$

where ρ stands for the mass density of the fluid, and $\mathcal{M}_{A,L}^0 = \delta v_L (4\pi\rho)^{1/2} / B_0$ the Alfvén Mach number at the large scale L with respect to the seed field intensity B_0 . Large turbulent Reynolds numbers result in faster SSDs, however the saturation occurs at lower amplification levels reducing its effectiveness. In the opposite

³ when the magnetic energy density is small compared to the kinetic energy density of the smallest turbulent scale

⁴ Here we define the Reynolds number as $Re = \delta v_L L/\nu$, being ν the fluid viscosity and L the largest turbulent scale. We also make use of the Kolmogorov scaling relation for the velocity $\delta v_l \propto l^{1/3}$

trend, relatively smaller values of Re result in slower SSDs, but with larger $B(t_{\text{sat}})$. However, in order to explain the cosmological amplification of magnetic fields after recombination era we need large $B(t_{\text{sat}})$ and fast amplification. During the formation of clusters of galaxies, starting at $z \sim 1.0$ (which represents a *look back time* of $< 8\text{Gyrs}^5$), velocities of the order of hundreds of km/s^6 are driven at scales as large as $L \sim 1\text{Mpc}$. For typical intergalactic gas densities of $n \sim 10^{-3}\text{cm}^{-3}$ one finds $B(t_{\text{sat}}) \sim \mu\text{G}$ for $Re \sim 10 - 1000$, which resembles the values expected for the IGM using the Spitzer viscosity. For a seed field $B_0 \lesssim \text{nG}$, using the same parameters, one also finds $t_{\text{sat}} > 10\text{Gyrs}$. It is clear, at least from these crude estimates, that only superestimated values of the magnetic seed field and a fine tuned Reynolds number could explain the magnetic field intensities observed in the local Universe (see e.g. Cho 2014).

Given the inefficient amplification of the field by the turbulent dynamo, another mechanism must be considered. It has been recently pointed that the IGM may not be well described by a standard MHD theory. The intergalactic plasma, extremely rarefied, behaves as a gyrotropic collisionless plasma, i.e. the Larmor radius of the ions ($r_L \sim eB/mc v_{\text{th},i}$) is smaller than the mean free path $\lambda_{\text{mfp}} \sim (n\sigma_{ii})^{1/2}$, being σ_{ii} the ion-ion collision cross-section (Schekochihin et al. 2005; Santos-Lima et al. 2014). This relation can be rewritten as the condition for gyrotropic plasmas as $B_{\text{gyro}}(\text{G}) \gtrsim 10^{-20} n(\text{cm}^{-3}) T(\text{eV})^{-1/2}$. In the standard ΛCDM Universe, with an average density of baryons at $z \sim 1000$ of $n_{z1000} \sim 10^6\text{cm}^{-3}$ and $kT_{z1000} \sim 1\text{eV}$, one finds $r_L < \lambda_{\text{mfp}}$ for magnetic fields larger than $\sim 10^{-14}\text{G}$, which decreases with time as the Universe expands. Therefore, for the given seed fields above, it is natural to assume the intergalactic plasma as gyrotropic. If not during its whole evolution post-recombination evolution, at least from the time when the condition $r_L < \lambda_{\text{mfp}}$ is satisfied.

Even in the fluid approximation (Chew et al. 1956, CGL-MHD hereafter) gyrotropic plasmas are subject to a number of instabilities that provide fast interchange of internal, kinetic and magnetic energies. Schekochihin & Cowley (2006a) presented a simplified analytical study of the time evolution of the magnetic energy in the ICM based on such instabilities. Their conclusion was that collisionless plasma instabilities may result in an “explosive” growth of magnetic energies in very short timescales compared to the cosmological evolution of the system. However, such idea has not yet been extended into a full theory nor tested numerically, which is the main goal of this work.

In the present paper we study numerically the amplification of magnetic fields in turbulent collisionless plasmas, under the CGL-MHD formalism. In order to achieve this goal we provide a number of direct numerical simulations of plasma flows, with forced turbulence, threaded initially by extremely weak seed fields. Collisionless plasma instabilities are included. The basic theoretical aspects of such problem is discussed in Section 2.

⁵ For a standard ΛCDM cosmological model, assuming a dark energy density $\Lambda = 0.714$, matter density (baryons + dark matter) $\Omega_M = 0.286$ and a Hubble parameter $h = 0.7$

⁶ as estimated from equipartition with thermal component, i.e. mildly transonic turbulence

The numerical setup and algorithms used are provided in Section 3. In Section 4 we present the main results, followed by the Discussions and the Conclusions.

2. MAGNETOHYDRODYNAMIC DESCRIPTION OF COLLISIONLESS PLASMAS

The proper description of collisionless plasmas relies on the full calculation of the particle dynamics, including both electromagnetic and collisional forces. Unfortunately such approach is of little practical use, with no analytical model available yet. One of the alternatives for this problem relies on numerically integrating the equation of motion of an ensemble of charged test particles (ions), coupled to a fluid (electrons). Such approach is also called particle-in-cell (PIC) numerical simulations. PIC simulations provide the dynamical evolution of momentum distributions of particles as they interact with magnetic fields and due to collisions, which allow us to directly study e.g. the effects of collisionless plasma instabilities on the isotropization of pressures, or on the rise of pressure anisotropies. However, the spatial coverage of the computational domain in PIC simulations is limited to a finite number of Larmor radii. For this reason it is not possible to study both the evolution of the distributions of particle momenta and the system dynamics at large scales, such in the case of the IGM, simultaneously. At first approximation, we may consider the distribution of momenta of particles to be Maxwellian (or bi-Maxwellian in the case of magnetized collisionless plasmas), for which a fluid description of a pressure-anisotropic plasma is available (Chew et al. 1956).

2.1. Single fluid approximation of a plasma with pressure anisotropy

The derivation of the CGL-MHD equations from the Vlasov-Maxwell equations is provided, for example, in Kulsrud (1983). By neglecting heat conduction and other possible heating/cooling sources, the one fluid CGL-MHD set of equations for a plasma with pressure anisotropy can be rewritten, in conservative form, as:

$$\frac{\partial}{\partial t} \begin{bmatrix} \rho \\ \rho \mathbf{u} \\ \mathbf{B} \\ e \end{bmatrix} + \nabla \cdot \begin{bmatrix} \rho \mathbf{u} \\ \rho \mathbf{u} \mathbf{u} + \Pi_P + \Pi_B \\ \mathbf{B} \mathbf{u} - \mathbf{u} \mathbf{B} \\ e \mathbf{u} + \mathbf{u} \cdot (\Pi_P + \Pi_B) \end{bmatrix} = \begin{bmatrix} 0 \\ \mathbf{f} \\ 0 \\ \mathbf{f} \cdot \mathbf{v} \end{bmatrix}, \quad (2)$$

where ρ , \mathbf{u} , \mathbf{B} , $p_{\perp,\parallel}$ represent the plasma density, velocity, magnetic field, and perpendicular/parallel pressures with respect to orientation of the local magnetic field, respectively, and $e = (p_{\perp} + p_{\parallel})/2 + \rho u^2/2 + B^2/2$ is total energy density. The anisotropy in pressure for a gyrotropic plasma is then defined as $\Delta \equiv (p_{\perp} - p_{\parallel})/p_{\perp}$. Π_P and Π_B are the pressure and the magnetic stress tensors, respectively, given as:

$$\Pi_P = p_{\perp} \mathbf{I} + (p_{\parallel} - p_{\perp}) \mathbf{b} \mathbf{b}, \quad (3)$$

and

$$\Pi_B = (B^2/8\pi) \mathbf{I} - \mathbf{B} \mathbf{B}/4\pi, \quad (4)$$

where \mathbf{I} is the unitary dyadic tensor and $\mathbf{b} = \mathbf{B}/B$. The source term \mathbf{f} , in the equations above, represents the external force responsible for driving the turbulence.

The set of equations given in Eq.2 is not closed. Since the perpendicular and parallel pressures can evolve differently from each other, another equation relating the time evolution of p_\perp and p_\parallel is needed. The original double-adiabatic condition proposed in Chew et al. (1956), based on the conservation of first and second magnetic invariants, leads to:

$$\frac{d}{dt} \left(\frac{p_\perp}{\rho B} \right) = 0, \quad \frac{d}{dt} \left(\frac{p_\parallel B^2}{\rho^3} \right) = 0. \quad (5)$$

The CGL-MHD double-adiabatic closure equations above may not be exactly correct. It is known that several processes, e.g. collisions or enhanced particle scattering by magnetic mirrors (or firehoses (e.g. Kunz et al. 2014)), break these invariants. Another possible closure for Eq.2 is obtained by simply assuming that the system reaches a pressure anisotropy equilibrium fast enough, so $\Delta = \text{const.}$ during the whole evolution. The closure problem is discussed in more details in the following sections.

2.2. Wave modes and stability condition in gyrotropic plasmas

A linear perturbation analysis of Eq.2 results in the known modified dispersion relations in gyrotropic plasmas given below (see e.g. Hau & Wang 2007; Kowal et al. 2011):

$$\left(\frac{\omega}{k} \right)_a^2 = \left(\frac{B^2}{4\pi\rho} + \frac{p_\perp}{\rho} - \frac{p_\parallel}{\rho} \right) \cos^2 \theta, \quad (6)$$

corresponding to the Alfvén transversal mode, with $\cos \theta = \mathbf{k} \cdot \mathbf{B}/(kB)$ (being \mathbf{k} the wavevector of the perturbation), and:

$$\left(\frac{\omega}{k} \right)_{f,s}^2 = \frac{b \pm \sqrt{b^2 - 4c}}{2}, \quad (7)$$

corresponding the fast (“+”) and slow (“−”) magnetosonic waves, being

$$b = \frac{B^2}{4\pi\rho} + \frac{2p_\perp}{\rho} + \left(\frac{2p_\parallel}{\rho} - \frac{p_\perp}{\rho} \right) \cos^2 \theta, \\ c = -\cos^2 \theta \left[\left(\frac{3p_\parallel}{\rho} \right)^2 \cos^2 \theta - \frac{3p_\parallel}{\rho} b + \left(\frac{p_\perp}{\rho} \right)^2 \sin^2 \theta \right].$$

The equations above result in the following stability conditions:

$$|\Delta| \equiv \frac{|p_\perp - p_\parallel|}{p_\perp} > 2\beta_\perp^{-1}, \quad \text{for } (p_\parallel > p_\perp), \\ \text{and} \\ \frac{1}{6} \frac{p_\perp}{p_\parallel} > 1 + \beta_\perp^{-1}, \quad \text{for } (p_\parallel < p_\perp) \quad (8)$$

which correspond to the firehose and fluid mirror instabilities, respectively. We must point out that there is a factor of 1/6 for the later, which is not present in the

threshold of the actual mirror instability obtained from the kinetic theory. This offset is a well-known issue in the CGL-MHD closure, but this is not relevant for this work as we focus on the evolution of the firehose mode only.

3. AN APPROXIMATE ANALYTICAL SOLUTION FOR THE AMPLIFICATION OF B IN THE UNSTABLE REGIME

By differentiating the pressure anisotropy Δ in time one obtains:

$$\frac{d\Delta}{dt} = \frac{1}{p_\perp} \left[(1 - \Delta) \frac{dp_\perp}{dt} - \frac{dp_\parallel}{dt} \right]. \quad (9)$$

The first term of the right side of Eq.9 can be evaluated in terms of the magnetic field intensity. The magnetic moment, or first adiabatic invariant, $\mu = m_i v_\perp^2 / 2B = \text{constant}$, of a charged particle subject to the magnetic force, is also quasi-invariant for a plasma. Therefore, by approximating v to the thermal velocity v_{th} , associated to the Maxwellian distribution of velocity components perpendicular to the magnetic field, and assuming $dp/\rho \ll dB/B$, we find $dp_\perp/p_\perp \simeq dB/B$, and Eq.9 results in:

$$\frac{d\Delta}{dt} \simeq (1 - \Delta) \frac{1}{B} \frac{dB}{dt} + \mathcal{F}_{iso}, \quad (10)$$

where

$$\mathcal{F}_{iso} = -\frac{1}{p_\perp} \frac{dp_\parallel}{dt} - \nu_{ii} |\Delta|, \quad (11)$$

represents an effective isotropization rate ($\nu_{eff} \sim \mathcal{F}_{iso} \Delta^{-1}$). Notice that the first term in the right hand side of the equation above corresponds to the time evolution of p_\parallel as a consequence of the changes in B and p_\perp . From here we describe the interchange of parallel and perpendicular pressures, mediated by magnetic fluctuations, as the net magnetic scattering of the particle distributions ($\nu_{scatt} \sim p_\perp^{-1} \Delta^{-1} dp_\parallel/dt$). The last term of the equation above has been deliberately added to account for the effect of collisions, by means of a Braginskii collision frequency ν_{ii} . From these two terms it is possible to consider two different regimes with: i) collision dominated isotropization, for $\nu_{ii} \gg \nu_{scatt}$; and ii) scattering dominated isotropization, for $\nu_{ii} \ll \nu_{scatt}$.

The effect of collisionless instabilities on the pitch angle (magnetic) scattering is not fully understood. If we take the firehose instability as example, perturbations (e.g. in the velocity field) may result in local growth of magnetic field intensity (δB). This in turn results in an increase of the perpendicular velocities of the ions, i.e. an increase of p_\perp , at the expense of a decrease of p_\parallel . This could in principle be used to estimate dp_\parallel/dt ⁷. However the total internal energy may not be conserved if particles are lost during scattering, or if other energy loss processes are included, making the problem not practical without a full kinetic description. An alternative, as pointed by Schekochihin & Cowley (2006b), is to assume this term to saturate the amplification of the magnetic field perturbations quasi-linearly at the wavelength of fastest growth, which occurs around the Larmor radius ($\omega \sim \Omega_i$,

⁷ e.g. as with the use of the 2nd adiabatic invariant

being $\Omega_{rmi} = eB/m_i c$ the cyclotron frequency of the ions) (Gary et al. 1998), therefore $\delta B/B|_{\text{sat}} \sim \gamma_{\text{max}} \Omega_i^{-1}$, given the maximum growth rate (see Eqs.6 and 7):

$$\gamma_{\text{max}} \sim \left(|\Delta| - \frac{2}{\beta} \right)^\alpha \Omega_i, \quad (12)$$

with $\alpha = 1$ and $1/2$ for mirror and firehose instabilities, respectively. As we show further in this paper the firehose instability is of major interest in the amplification of B , and we use $\alpha = 1/2$ from here. The scattering frequency can then be estimated as $\nu_{\text{scatt}} \simeq \delta B^2/B^2 \gamma_{\text{max}} \sim (|\Delta| - 2/\beta)^{3/2} \Omega_i$, and Eq.10 becomes:

$$\frac{d\Delta}{dt} \sim (1 - \Delta) \frac{1}{B} \frac{dB}{dt} + \left(|\Delta| - \frac{2}{\beta} \right)^{3/2} \Omega_i - \nu_{ii} |\Delta|. \quad (13)$$

3.1. Magnetic field amplification with constant Δ

This problem is tractable analytically if we assume that the evolution of the firehose unstable regions in the plasma occur with constant Δ . This approximation is justified by the fact that any process that may amplify the pressure anisotropy (e.g. turbulence, anisotropic cosmic ray scattering, and others) is precisely counterbalanced by the ones leading to isotropization. This is actually a probable scenario given that the increase of the pressure anisotropy by external sources is independent on Δ , while the isotropization processes are a function of the anisotropy itself. Therefore, the system should evolve around an “equilibrium” anisotropy value Δ_0 . If the relaxation timescale is short compared to the dynamical timescales of the system, we may assume $\Delta(t) \simeq \Delta_0$. We must stress that the validity of such conjecture depends on the level of anisotropy itself, i.e. it is probably correct for $\Delta_0 \rightarrow 0$ and certainly does not stand for $\Delta_0 \gg 0$.

3.1.1. the case of $\nu_{ii} \gg \nu_{\text{scatt}}$

Let us first consider the case in which collisions dominate the isotropization of pressure. This limit could well describe the initial stages of the evolution of a cosmological seed field after the recombination era, given that $\beta \gg 1$ and $\nu_{ii} \gg \Omega_i$. The evolution of the magnetic field in this case depends mostly on the dynamics of the plasma, and not on instabilities driven by the pressure anisotropy. Given that the resistive dissipation is extremely small in the intergalactic medium we may apply the “frozen-in” condition to the plasma. The evolution of the magnetic field is then dominated by the turbulent rate of strain at the viscous scales (see e.g. Schekochihin & Cowley 2006b):

$$\frac{1}{B} \frac{dB}{dt} \simeq \mathbf{b} \mathbf{b} \cdot \nabla \mathbf{u} - \nabla \cdot \mathbf{u} \sim \frac{\delta v_L}{L} Re^{1/2}. \quad (14)$$

For $\Delta = \text{const}$ and $\nu_{ii} \gg \nu_{\text{scatt}}$, and combined with Eq.14, Eq.13 is then reduced to:

$$|\Delta| \sim \left(\frac{v_{\text{th}}}{\delta v_L} \right)^{3/2} \left(\frac{L}{\lambda_{\text{mfp}}} \right)^{1/2} - 1. \quad (15)$$

As discussed in the previous section the kinetic phase of the turbulent dynamo (Eq.14) provides an exponential growth of the seed field up to equipartition at the

smallest turbulent scales. However, as B grows, $\Omega_i \rightarrow \nu_{ii}$ and the plasma becomes gyrotropic. This is supposed to occur for extremely weak magnetic fields ($B_{\text{gyro}}(\text{G}) \gtrsim 10^{-20} n(\text{cm}^{-3}) T(\text{eV})^{-1/2}$), possibly even earlier than the saturation of the turbulent dynamo at small scales.

Another interesting aspect of the turbulence during the early evolutionary phase is to generate the pressure anisotropy by itself (Eq.15). This is physically understood as the consequence of a fast growth of the magnetic field not counterbalanced by collisions. Depending on the properties of the turbulence, one obtains $|\Delta| \gg 0$. Such values are not expected in highly magnetized plasmas. Once $\nu_{ii} \ll \nu_{\text{scatt}}$, due to the amplification of B , the balance is reached since ν_{scatt} strongly depends on the magnetic field intensity. Local measurements of the Earth’s magnetosphere and the solar wind reveal pressure anisotropies around its quasi-stability threshold $|\Delta| \sim |\Delta|_{\text{crit}}$, and many signatures of its role on the dynamical evolution of these systems have been found (e.g. Winterhalter et al. 1995; Soucek et al. 2008; Bale et al. 2009). The interesting implication of Eq.15 is that, due to its lower magnetization level (much higher β), $|\Delta|$ in the IGM/ICM could have been much larger at higher redshifts, compared to the values found presently in the Solar System.

3.1.2. the case of $\nu_{ii} \ll \nu_{\text{scatt}}$

Once the magnetic field becomes strong enough, for the plasma to become gyrotropic, instabilities will take over the amplification of the magnetic field. Now, as $\Delta = \text{const}$ and $\nu_{ii} \ll \nu_{\text{scatt}}$, and replacing the cyclotron frequency Ω_i , Eq.13 becomes⁸:

$$\frac{dB}{dt} \sim \frac{e}{m_i c} \frac{(|\Delta| - 2\beta^{-1})^{3/2}}{1 + |\Delta|} B^2, \quad (16)$$

which, at $\beta \gg |\Delta|^{-1}$ limit, result in a first order non-linear ordinary differential equation with an analytical solution:

$$B(t) \sim (B_0^{-1} - At)^{-1}, \quad (17)$$

with $A \simeq \frac{e}{m_i c} \frac{|\Delta|^{3/2}}{1 + |\Delta|}$. The magnetic field growth is explosive around $t \sim A^{-1}$, and the saturation occurs for $B(\tau_{\text{gr}}) \gg B_0$. The quasi-stability condition, given by $\beta \sim 2/|\Delta|$ level, is reached in a timescale:

$$\tau_{\text{gr}}(s) \sim (|\Delta|^\psi \Omega_{i,0})^{-1} \sim 10^{-4} B_0^{-1}(\text{G}) |\Delta|^{-\psi}, \quad (18)$$

where $\Omega_{i,0}$ represents the cyclotron frequency measured for the seed field B_0 , and $\psi = 1/2$, or $3/2$, for $|\Delta| \gg 1$ and $|\Delta| \ll 1$, respectively. Eq.18 then provides an approximate timescale for the explosive growth of the magnetic field due to the collisionless plasma instability. For example, if we consider a seed field of $B_0 \sim 10^{-17} \text{G}$ subject to such instabilities, with $|\Delta| > 10^{-2}$, one finds amplification up to equipartition with pressure anisotropy ($\beta \sim |2\Delta|^{-1}$) at $t < 400 \text{Myrs}$.

⁸ notice that the amplification of B in our model can occur for firehose instability, i.e. $p_{\parallel} > p_{\perp}$ (see Eq.9), and therefore $\Delta < 0$ and $1 - \Delta > 1$

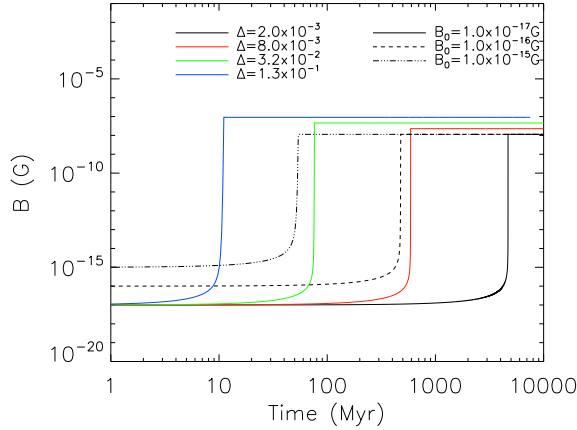


FIG. 1.— Time evolution of magnetic field amplitude in the approximate case of Eq.16, as described in Section 3.1.2.

As pointed before, such values of pressure anisotropies are easily reached in turbulent weakly magnetized collisionless plasmas. The main conclusions of this section are that: i) pressure anisotropies could be naturally generated in the IGM/ICM in the early Universe (post-recombination era) at timescales comparable to the eddy turnover time at viscous dissipation scales, and ii) the instabilities driven by the pressure anisotropy. A full numerical integration of Eq.16 is shown in Figure 1, which confirms the main results obtained in the approximate limits $\beta \gg |\Delta|^{-1}$ and $B(\tau_{\text{gr}}) \gg B_0$.

4. NUMERICAL SIMULATIONS

In the previous section we demonstrated that the evolution of plasma instabilities driven by a pressure anisotropy could, in principle, explain the amplification of a magnetic field seed at recombination era to the values observed in the local Universe. These estimates, however, were obtained under strict approximations and limit cases. In this section we describe the numerical methods used for modelling of the dynamical evolution of the unstable plasmas.

4.1. Governing equations and methods

In order to perform the numerical modeling of the plasma evolution with the constant pressure anisotropy and turbulence injection we used the GODUNOV code⁹ which solves the CGL-MHD equations (Eqs. 2) in the conserved form.

For simplicity $p_{\parallel} = a_{\parallel}^2 \rho$ and $p_{\perp} = a_{\perp}^2 \rho$ are expressed by the sound speeds a_{\parallel} and a_{\perp} , parallel and perpendicular to \mathbf{B} , respectively. Therefore the momentum equation can be rewritten as

$$\frac{\partial \rho \mathbf{u}}{\partial t} + \nabla \cdot \left[\rho \mathbf{u} \mathbf{u} + \left(a_{\perp}^2 \rho + \frac{B^2}{8\pi} \right) \mathbf{I} - (1 - \alpha) \frac{\mathbf{B} \mathbf{B}}{4\pi} \right] = \mathbf{f}, \quad (19)$$

where $\alpha = (a_{\parallel}^2 - a_{\perp}^2)/V_A^2 = \frac{1}{2}(\beta_{\parallel} - \beta_{\perp}) = \frac{1}{2}\beta_{\perp}(\xi - 1)$ is the pressure anisotropy degree with $\xi \equiv p_{\parallel}/p_{\perp} = a_{\parallel}^2/a_{\perp}^2$ being the pressure ratio.

⁹ The MHD version of the code is publicly available from the website <http://amunocode.org>

The numerical integration of the modified¹⁰ CGL-MHD equations, was done in GODUNOV using the second-order shock-capturing Godunov-scheme (see Kowal et al. 2011). The time integration was done using the second order Strong Stability Preserving Runge-Kutta (SSPRK) method (see Gottlieb et al. 2009, and references therein). Spatial reconstruction was done using the second order the total variation diminishing (TVD) interpolation with the Van Leer limiter (van Leer 1974), and numerical fluxes were calculated using the general Harten-Lax-van Leer (HLL) Riemann solver (see Einfeldt 1988, e.g.). We incorporated the field interpolated constrained transport (CT) scheme (see Tóth 2000, e.g.) into the integration of the induction equation to maintain the $\nabla \cdot \mathbf{B} = 0$ constraint numerically.

4.2. Model of turbulence

In our numerical modeling we drive turbulence using a method described by Alvelius (1999). The forcing is implemented in spectral space and concentrated around the injection scale related to a wave vector k_{inj} . We perturb a finite number of discrete Fourier components of velocity in a shell extending from $k_{inj} - \Delta k_{inj}$ to $k_{inj} + \Delta k_{inj}$ with a Gaussian profile of the half width k_c and the peak amplitude \tilde{v}_f at the injection scale. The amplitude of driving is solely determined by its power P_{inj} . The parameters describing our forcing do not change during the evolution of the system.

The randomness in time makes the force neutral in the sense that it does not directly correlate with any of the time scales of the turbulent flow, and it also determines the power input solely by the force-force correlation. In the models presented in this paper we use isotropic forcing.

In particular, the total amount of power input from the forcing can be set to balance a desired dissipation at a statistically stationary state. In order to contribute to the input power in the discrete equations from the force-force correlation only, the force is determined so that the velocity-force correlation vanishes for each Fourier mode. The procedure of reducing the velocity-force correlation is described in Alvelius (1999).

In Eq. (19), the forcing is represented by a function $\mathbf{f} = \rho \mathbf{a}$, where ρ is local density and \mathbf{a} is random acceleration calculated using the method described above.

4.3. Initial and boundary conditions

For our calculations, similar to our earlier studies (see Kowal et al. 2011), the initial pressures and the uniform initial field B_0 are the controlling parameters. We define the Alfvénic Mach number of the injected turbulence as $\mathcal{M}_A = \langle \delta v / c_A \rangle$. The angle brackets $\langle \rangle$ represent the volume average of the parameter.

The distribution of $\rho = 1.0$, $\mathbf{v} = 0$ and $\mathbf{B} = B_0 \hat{\mathbf{x}}$, is uniform in the whole domain. We do not set the viscosity nor the resistivity coefficients explicitly in our models, and dissipation is determined by the numerical scheme only. Therefore the scales at which the dissipation starts to be important is defined by the numerical diffusivity of the scheme.

¹⁰ standard solution of CGL-MHD equations involves the use of the first and second adiabatic invariants as closures for the problem. Here, this is slightly modified as we avoid the use of the 2nd adiabatic invariant by fixing the pressure anisotropy as constant.

TABLE 1
INITIAL AND SATURATION PROPERTIES OF THE NUMERICAL SIMULATIONS

model	res	$\mathcal{M}_{A,0}^a$	β_0	p_\perp	p_\parallel	$ \Delta ^b$	$\langle \beta^{\text{sat}} \rangle$	$\tau_{\text{sat}}(t_{\text{dyn}})$
fh512Ma0D1.0	512 ³	2.0	2.0	0.25	1.0	3.0	1.6	0.52
mr512Ma0D0.5	512 ³	1.0	3.0	4.0	1.0	0.75	4.3	-
mr256Ma4D0.8	256 ³	10 ⁴	6.8×10^7	1.0	0.04	0.96	2.5×10^7	-
mr256Ma4D0.6	256 ³	10 ⁴	7.5×10^7	1.0	0.25	0.75	2.2×10^7	-
fh512Ma4D1.0	512 ³	10 ⁴	2.0×10^8	1.0	4.0	3.0	7.6	0.36
fh256Ma4D1.0	256 ³	10 ⁴	2.0×10^8	1.0	4.0	3.0	7.8	0.62
fh128Ma4D1.0	128 ³	10 ⁴	2.0×10^8	1.0	4.0	3.0	7.9	1.40
fh256Ma4D4.0	256 ³	10 ⁴	9.0×10^8	1.0	25.0	24.0	1.4	0.13
fh256Ma4D9.0	256 ³	10 ⁴	3.4×10^9	1.0	100.0	99.0	0.6	0.07
fh256Ma6D4.0	256 ³	10 ⁶	9.0×10^{12}	1.0	25.0	24.0	1.3	0.18
fh256Ma8D4.0	256 ³	10 ⁸	9.0×10^{16}	1.0	25.0	24.0	1.4	0.22

^a $\mathcal{M}_{A,0} = \delta V^{\text{inj}}/V_{A,0}$ is the Alfvén Mach number of the turbulence injected with respect to the initial magnetic field, i.e at $t = 0$

^b $\Delta = (p_\perp - p_\parallel)/p_\perp$

The simulation box is perfectly periodic in all directions.

4.4. Simulated models

For the present work we performed a number of numerical simulation with different plasma initial parameters, as well as different stability regimes, as given in Table 1. We also performed simulations varying the numerical resolutions for the purpose of convergence validation.

5. RESULTS

A comparison between the spatial distributions of the density and velocity fields in CGL-MHD and standard MHD turbulent models have been provided in Kowal et al. (2011) and Santos-Lima et al. (2014). In those works it has been shown that CGL-MHD models, depending on the filling factor of unstable regimes and on the degree of pressure anisotropy itself, may lead to evident differences in the statistics of turbulent fields when compared to standard MHD turbulence. Those studies were performed for relatively strong magnetic fields, i.e. for $p_\perp |\Delta| \gtrsim \langle B^2 \rangle$, and therefore the statistics of \mathbf{B} were weakly dependent on CGL-MHD instabilities (see Fig.6 in Santos-Lima et al. 2014). Differently to the previous works, we focused our modelling on the weakly magnetized turbulent regimes ($p_\perp |\Delta| \gg \langle B^2 \rangle$).

5.1. Magnetic field structure and statistics

As the simulations are initiated, the driving of turbulence results in fluctuations of density, and of the velocity and magnetic fields, at different scales. It is well known for many decades that firehose and mirror instabilities, given the growth rate dependence with k (Eqs.6 and 7), result in the emergence of structures much smaller than those observed in standard MHD turbulence (Kowal et al. 2011). In standard MHD, the forcing, i.e. the process of injection of turbulence, is the dominant dynamical process and therefore dominate the process of structure formation. In the collisionless plasma approximation, on the other hand, the growth rate of the instabilities rises indefinitely with the wavenumber of the fluctuation, up to $k_{\text{max}} \sim r_L$. The numerical scheme implemented in this work for solving the CGL-MHD equations do not account for finite Larmor radius effects. Therefore, the maximum growth rate of the instabilities must be related to the minimum lengthscales of the system,

which is the size of the finite volume of the space discretization, i.e. the grid cell. This means that both the growth rate and the geometry of the amplified magnetic fields are resolution dependent.

In Figure 2 we present the apparent configuration of the magnetic field lines in the mid-slice (in the z -direction). The geometry of the field lines is illustrated by the line integral convolution (LIC) technique. The LIC imaging algorithm consists of rendering a map of random streamlines that follow the orientation of the local field. The values are normalized to arbitrary units in order to provide a texture map. Such texture map provides a visual qualitative measure for the scaling of the magnetic field lines. Figure 2 shows the LIC technique applied for the the magnetic field lines at saturated stage for $|\Delta| = 3.0$ and $\beta_0 = 2 \times 10^8$, corresponding to firehose unstable models, for the given resolutions of 128³ (left), 256³ (center) and 512³ (right).

It is visually clear from these plots that the finer the resolution the more flocculent the geometry of the amplified magnetic field becomes. This result is expected since for $|\Delta| = 3.0$ and $\beta_0 = 2 \times 10^8$ models the thermal pressure, including the pressure anisotropy free-energy, is much larger than the magnetic and turbulent driving energy densities. Therefore the firehose instability dominates the plasma dynamics and the structure formation, which growth rate should peak around the smallest scales available in the system. This is also quantitatively measured by means of the normalized power spectrum of the magnetic field, shown in Figure 3 (top). The three dimensional power spectra of the magnetic field for these models reveal that the peak shifts towards larger k 's as the numerical resolution increases. The peak shift is linear with the resolution, occurring at rounded values of $k_{\text{peak}} \simeq 16, 33$ and 65 , for resolutions of 128³ (black), 256³ (red) and 512³ (blue), respectively. Perturbations smaller than 6 – 8 grid cells suffer mostly the effects of numerical dissipation.

Notice that, theoretically, the maximum growth rate should occur at $k \sim k_{\text{peak}}$ but numerical diffusion is responsible for the dissipation of coherent structures at the smallest scales. Both the numerical viscosity and resistivity act together to reduce the effect of the instabilities in the growth of velocity and magnetic field perturbations. If the numerical viscosity is considered to be Laplacian we can, in principle, estimate the peak

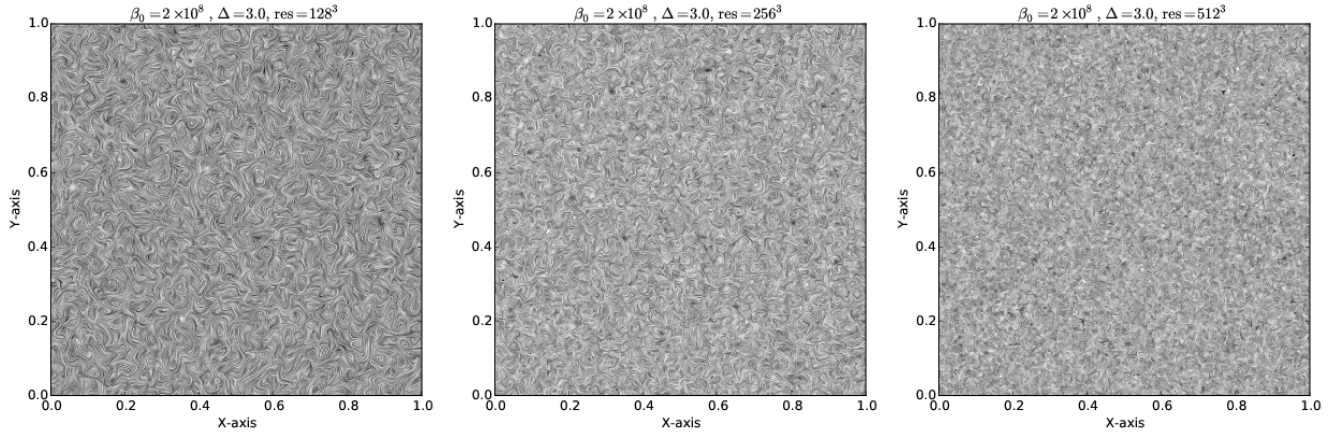


FIG. 2.— Central slice line integral convolution (LIC) map of the magnetic field lines at saturated stage for $|\Delta| = 3.0$ and $\beta_0 = 2 \times 10^8$, firehose unstable, models with different resolutions: 128^3 (left), 256^3 (center) and 512^3 (right).

location as the lengthscale at which the numerical viscous loss rate ($4\pi^2 k_{\text{peak}}^2 \nu_{\text{num}}$) equals the instability growth rate, which results in $k_{\text{peak}} \sim \sqrt{|\Delta| - 2\beta^{-1}} (8\pi^3 \nu_{\text{num}})^{-1}$. Given that the asymptotic values of β depends only on Δ , when saturation of instabilities occurs the peak location becomes insensitive to $(|\Delta| - 2\beta^{-1})$, resulting in $k_{\text{peak}} \propto \nu_{\text{num}}^{-1}$, i.e. approximately linearly proportional to the numerical resolution as suggested before.

Also, it is noticeable that the numerical resolution, except for the location of the peak, is not relevant for the general shape of the power spectrum of the magnetic field fluctuations. A power spectrum $P \propto k^\alpha$, with $\alpha \sim 2$, is observed in the range of scales $\sim [k_{\text{inj}}, k_{\text{peak}}]$, in agreement with the saturation estimates for $\delta B_k^2 \propto \gamma_k^2 \propto k^2$ (see Section 3), for all the numerical resolutions. This is a good indicative of convergence for the models. The obtained power spectrum is steeper than the one expected for the kinetic-phase of the small-scale dynamo, which shows that the instabilities are the dominant process in the field amplification here. This also show that the magnetic field at large scale is comparatively weaker.

The effects of $|\Delta|$ on the structure of the magnetic field is also shown in Figure 3 (center). Here we present the spatial spectral power of the magnetic field for the 5 different models with same thermal perpendicular pressure (p_\perp) and numerical resolution (256^3), at $t = 2.0t_{\text{dyn}}$, but for different parallel pressures (p_\parallel), resulting in mirror (“M”) and firehose (“FH”) unstable systems with different anisotropies. The mirror unstable models, in contrast to the firehose unstable ones, present a decreasing power with wavenumber. This is because, as shown above, the amplification of the magnetic fluctuations in the firehose regime is dominated by the instabilities (positive slope of the power spectra), while in the mirror unstable regions it is basically subject to the dynamics of the flow, i.e. the turbulence (responsible for the negative slope of the power spectra). Also, as we discuss in more details in the next subsection, the amplitude of the power spectrum is a function of the pressure anisotropy for the firehose unstable models, while it is insensitive to $|\Delta|$ in the mirror unstable models. In the firehose case, the larger the anisotropy the larger is the total power of the magnetic fluctuations, which is related to the real values of the fluctuations and to the degree of amplification itself.

Since saturation is an important condition for the identification of the peak and total power of the magnetic fluctuations we studied the time evolution of the spatial power spectrum of \mathbf{B} of one of the firehose unstable models ($|\Delta| = 24, \beta_0 = 9 \times 10^{16}$ and 256^3). We chose the model with the smallest magnetic seed field given its longer saturation timescale, which could eventually influence the spectral power distribution. As can be seen from Figure 3 (bottom), the spectra are very similar for all snapshots ($t = 0.5, 1.0, 1.5$ and $2.0t_{\text{dyn}}$), with exactly the same slopes and peak locations. This means that the saturation occurs at $t \ll t_{\text{dyn}}$, and that the turbulence driven - even though super-Alfvénic (with respect to the seed field) - is not able to modify the spatial distribution of the amplified field fluctuations. It is worth mentioning here that, since the non-linear regime (as for the small-scale dynamo) apparently does not exist, another mechanism is therefore required to continue the magnetic field amplification on larger scales.

5.2. Magnetic field amplification

As indicated by the power spectra shown in Fig.3, the firehose unstable models result in amplified magnetic field fluctuations. In the left panel of Fig.4 we present time evolution of the magnetic energy density for models with different pressure anisotropy ratios. The magnetic energy density was averaged over all grid cells of the simulated box. As mentioned above, the mirror unstable models show moderate growth rates for the magnetic field perturbations, which occur at timescales of $\sim t_{\text{dyn}}$, in agreement with a typical slow turbulent dynamo. The firehose unstable models on the other hand present much larger amplification values, corresponding to > 7 orders of magnitude for the three models shown. Also, the amplification timescales are much shorter than in the mirror unstable case, with $\tau_{\text{gr}} \ll t_{\text{dyn}}$. For these models the saturation of magnetic energy density occurs at larger levels for larger pressure anisotropies, as expected for the saturation threshold $\beta_{\text{sat}}^{-1} \propto |\Delta|$ (see Eq.16). Also, in qualitative agreement with Eq.18, the saturation timescales for the magnetic field amplification decreases with pressure anisotropy. The timescales and amplification levels for saturation are also presented in Table 1.

Another interesting feature related to the time evolution of the magnetic energy density is the presence of a “knee” separating two different growth regimes. The

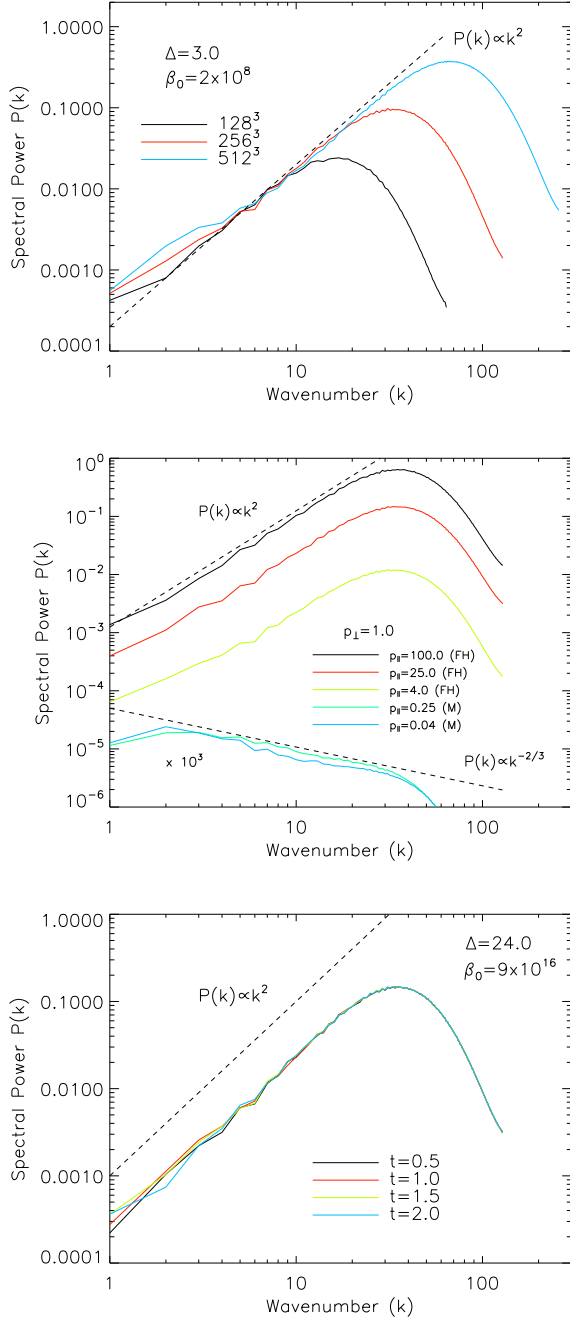


FIG. 3.— Spatial power spectra of the magnetic field for: different numerical resolutions (top), different pressure anisotropies (center), and at different stages of the system evolution (bottom).

energy density level of the knee is similar for all models. As pointed in Section 3, if the turbulent rate of strain is larger than the growth rate of the instabilities the turbulent dynamo regime dominates. This is precisely the physical motivation of the knee. At the early stages turbulence is driven at large scales, which are related to small growth rates of the instabilities. At this point Eq.14 is not yet valid given that the turbulence is not fully evolved, but could be replaced with a reduced effective Re number instead due to the shorter inertial range. The actual magnetic growth rate, related to the rate of strain, increases with time as the cascade develops and the inertial range grows. This behavior is also

observed in the curves of magnetic energy density evolution. Once perturbations grow at a particular scale, at which the growth rate of the instabilities take over the numerical dissipation, the explosive amplification takes place.

The right panel of Fig.4 presents the time evolution of the turbulent Alfvénic Mach number for the different models. All models start with similar turbulent strengths. From this it is clear that, for the cases with $\Delta < 0$, the bulk of the magnetic field amplification is not related to the turbulence itself (though it is needed to seed the fluctuations that are subject to the instabilities at a later stage). The mirror unstable models demonstrate very similar evolutions while, on the other hand, the firehose unstable models show different evolution depending on the level of pressure anisotropy. Again, as pointed before, the larger the pressure anisotropy the faster the plasma reaches saturation.

The same study is presented in Fig. 5, but for the different numerical resolutions. We can observe that the evolution of the average magnetic energy density and the Alfvénic Mach number present similar profiles for the different models. Therefore, the overall time dependency function of these quantities is well converged in our models. The convergence is good for the asymptotic value of the average magnetic energy density as well, which saturates for similar values regardless the resolution and depends on Δ exclusively. The timescales for saturation however is resolution dependent, as we have pointed previously, being shorter for higher resolutions. This is in agreement to the fact that finer resolutions allow the growth of the shorter wavelength perturbations, which have faster growth rates.

The effect of the seed field intensity on the magnetic growth rate is shown in Fig.6, for the models with $\Delta = 24.0$ and numerical resolution of 256^3 cells. Here the different seed field intensities correspond to initial thermal to magnetic pressure ratios $\beta_0 = 9 \times 10^{12}$ (red) and $\beta_0 = 9 \times 10^8$ (black). The time evolution of the Alfvénic Mach number (right panel) shows that saturation occurs at similar levels regardless of the seed field intensity. The saturation occurs once instabilities drive the amplification to $\sim |\Delta|p_\perp$ level, as predicted from the CGL-MHD stability condition. Weaker initial magnetic fields result in later saturation timescales. The delay, compared to the models with stronger initial fields, occurs as the road up to the saturation level must take longer for weaker seed fields.

Notice that the “knees”, i.e. the transition between the turbulent and instability driven dynamos, occur at similar times ($t \sim 0.02 - 0.03 t_{\text{dyn}}$) regardless the initial magnetic field intensity. Also, the magnetic field amplification, relative to the seed field intensity, of the knee is similar in the three models. Both features are in agreement to Eq.14. That equation reveals that, for the same timescales and similar turbulent properties, the relative amplification $\Delta B/B$ should be similar for all models.

The time evolution of the minimum and maximum magnetic energy densities are also shown in the left panel of Fig.6, as dashed lines. These follow qualitatively the same profiles of the mean magnetic energy density, except for the short period before the “knee”, when the maximum energy increases while the minimum energy decreases with time. This process is due to the tur-

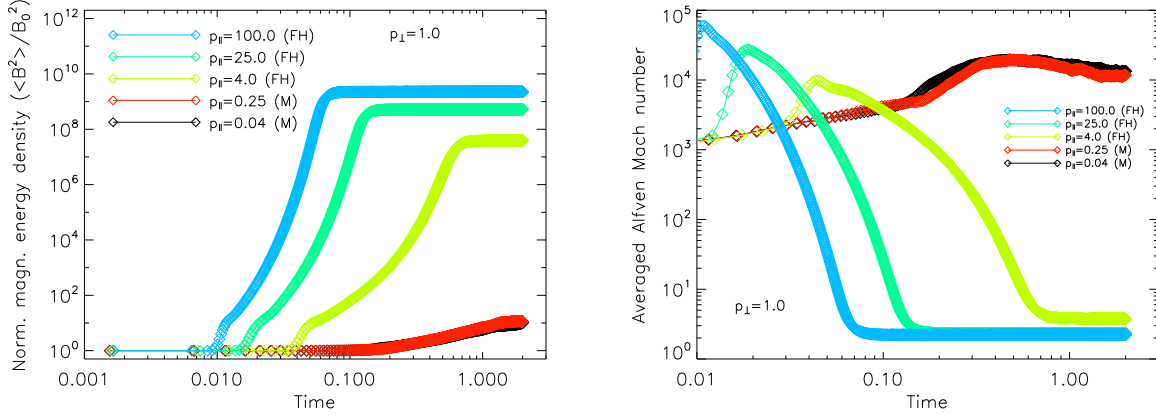


FIG. 4.— The time evolution of the magnetic energy density normalized by its initial value (left) and of the Alfvénic Mach number (right). The data shown correspond to the models with $p_\perp = 1.0$, 256^3 resolution, but $p_\parallel = 100.0$ (blue), 25.0 (green), 4.0 (yellow), 0.25 (red) and 0.04 (black).

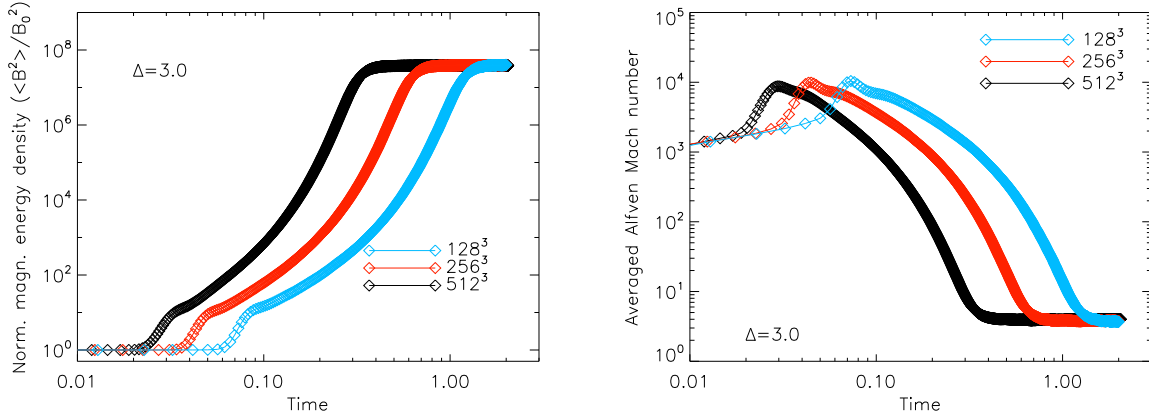


FIG. 5.— Same as Figure 4 but for the models with $\Delta = 3.0$, $\beta_0 = 2 \times 10^8$, and different resolutions: 128^3 (blue), 256^3 (red) and 512^3 (black).

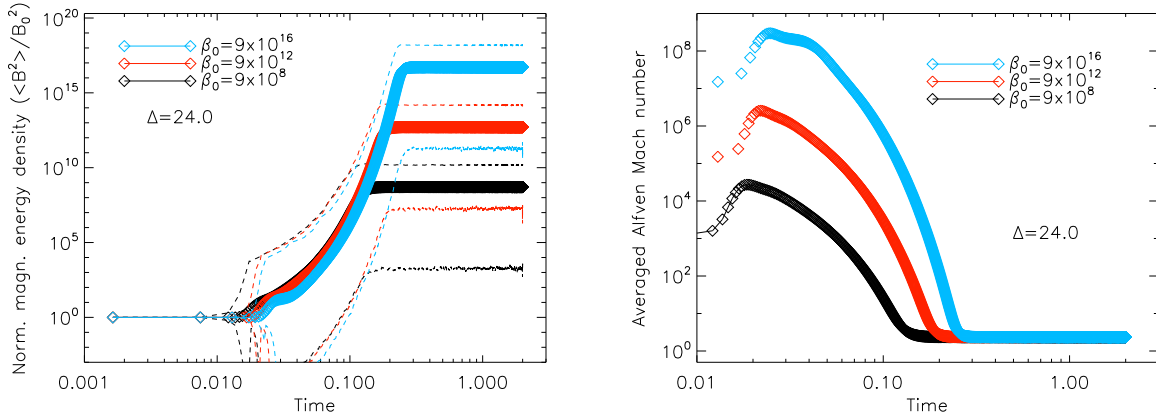


FIG. 6.— Same as Figure 4 but for the models with $\Delta = 24.0$, 256^3 resolution, and different seed fields: $\beta_0 = 7 \times 10^{16}$ (blue), $\beta_0 = 9 \times 10^{12}$ (red) and $\beta_0 = 9 \times 10^8$ (black).

bulence that increases the dispersion of the magnetic field distribution, before the growth of the instabilities. The second phase happens when the instability growth rate becomes more important than the turbulent rate of strain, therefore the “knee” occurs earlier for the maximum value curve (larger rate of strain), and later for the minimum value curve (lower rate of strain).

The turbulent broadening of the magnetic energy density is clearly seen in the probability distribution function (PDF) shown in Fig.7. In the left panel we present the PDFs as they depend on the pressure anisotropy. We show the models with $p_{\perp} = 1.0$, 256^3 resolution, for $p_{\parallel} = 100.0$ (black), 25.0 (red), 4.0 (yellow), 0.25 (green) and 0.04 (blue), all at $2.0t_{\text{dyn}}$. All models start with a delta function PDF, at $B/B_0 = 1.0$. The broadening observed in the mirror unstable models exemplifies the role of the injected turbulence on the distribution of the magnetic energy over the simulated domain. There is clearly no net amplification of the averaged field intensity though. The firehose unstable models present PDFs that are shifted and skewed. Not only the averaged field intensity is amplified, as discussed above, but these PDFs - as a whole - are shifted towards larger intensities, being the shift proportional to the pressure anisotropy.

The skewness of the PDFs arises as their peaks are further shifted towards larger intensities, compared to the bulk of the distribution. This occurs if the amplification of the magnetic field is larger/faster for stronger fields. Such behavior could be understood as a transient process due to the turbulent broadening, in which turbulence would naturally build-up strong field in more regions as time evolves, but this is not the case. The mirror unstable models do not present similar skewness. Also, the time evolution of the PDFs do not support such possibility. In the right panel of Fig.7 we show the time evolution of the PDF of magnetic field intensity for a single model. We have selected the model with 128^3 resolution because it presents the slower evolution of the distribution, and the PDFs obtained at different snapshots can be compared. Here we show four PDFs calculated at $t = 0.5, 1.0, 1.5$ and $2.0t_{\text{dyn}}$. The general PDF profiles change slightly with time, but is similarly skewed from $t = 0.5t_{\text{dyn}}$ up to saturation time. The aparent constant skewness of these curves shows that the changes in the distribution of magnetic field intensity occurs too early to be accounted for the turbulence, and should be related to the instability itself. This is in agreement with Eq.16, which predicts faster amplification for stronger fields.

5.3. Comparison to the analytical approximations

Obviously, any comparison between the simulations presented here and the magnetization of the intergalactic medium needs caution. The numerical simulations presented here correspond to full three-dimensional and stochastic numerical solutions of the problem. It represents a good benchmark for the analytical estimates (and approximations related) of the simplest zero-dimension, constant- Δ , $\beta \rightarrow \infty$ limit, derived in Section 3.

We start analysing the dependency of the saturation timescale observed in the simulations with the pressure anisotropy ratio (Δ). In the top panel of Fig.8 we present the values obtained from the simulations, as described in Table 1, together with a number of analytical solutions for comparison, as given by Eq.16. The trian-

gles represent the three models with similar parameters except for the pressure anisotropy, therefore we fit the analytical solutions to these data. The squares correspond to the models with different initial conditions and are included for the sake of comparison only. Here we also consider the fact that the simulated instabilities are slightly delayed by the fact that we do not initiate the models with fully developed turbulence. On the contrary, the initial configuration is that of an uniform magnetic field, which is disturbed as turbulence injected at large scale cascades. This turbulent delay (δt_{turb}) is introduced as a free constant parameter, i.e. $\tau_{\text{gr}} \sim t_{\text{sat}} - \delta t_{\text{turb}}$. Overall there is reasonable agreement between the simulations and the analytical solutions, being those with $0.01t_{\text{dyn}} < \delta t_{\text{turb}} < 0.05t_{\text{dyn}}$ particularly good. It is interesting to note that this range is similar to the timescales of the “knees” observed in Fig.4.

In the lower panel of Fig.8 the same study is presented but now for the initial values of the seed fields. Here the triangles represent the three models with similar initial conditions except for the seed field ($\beta_0 = 9 \times 10^8$, 9×10^{12} , and 9×10^{16}). According to Eq.18, the best fit to the data should occur for $\tau_{\text{gr}} \propto B_0^{\vartheta}$, with $\vartheta = -1.0$. However, as clearly seen from the plot, the best fits occur for a much weaker dependence (or even no-dependence) of τ_{gr} with the initial seed field, being $\vartheta \sim -0.05$. The apparent discrepancy between the two results is not real though. Notice that Eq.18 is derived as the magnetic field evolution once the condition $\nu_{\text{ii}} \ll \nu_{\text{scatt}}$ is fulfilled. The term B_0 is therefore somewhat misleading in the sense that one must consider the magnetic field intensity once $\nu_{\text{ii}} \ll \nu_{\text{scatt}}$, i.e. a transition field intensity. For the analytical model the transition field intensity is determined by ν_{ii} , while in the simulations by the numerical dissipation, i.e. in both cases it is insensitive to initial magnetic field. Another major effect responsible for this discrepancy is that fact that the growthrate depends on the Larmor radius, which cannot be properly modelled in the simulations. Naturally, τ_{gr} obtained from the simulations is overestimated as B increases with time.

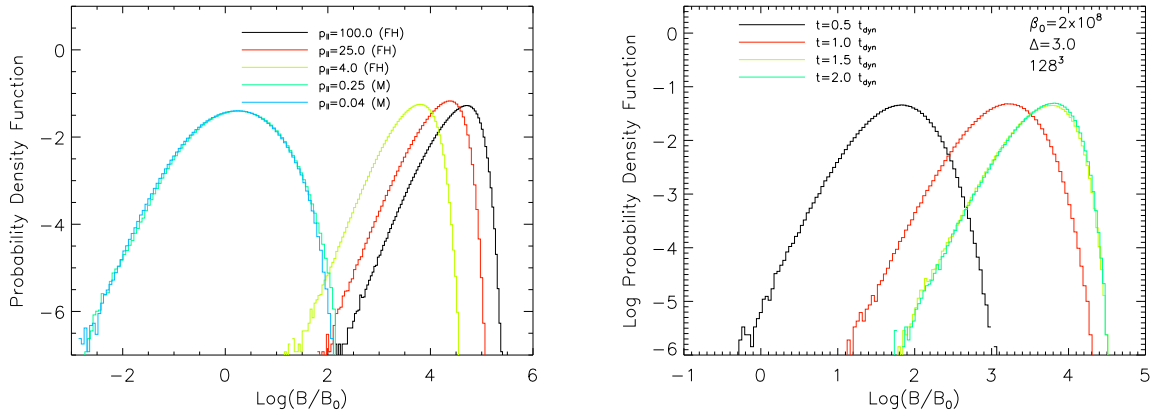


FIG. 7.— Probability distribution functions (PDFs) of the magnetic field intensity, normalized by its initial value, computed from all grid cells. *Left*: for the models with different pressure anisotropies, at $2.0 t_{\text{dyn}}$. The data represent the models with $p_{\perp} = 1.0$, 256^3 resolution, but $p_{\parallel} = 100.0$ (black), 25.0 (red), 4.0 (yellow), 0.25 (green) and 0.04 (blue). *Right*: for the $\beta_0 = 2 \times 10^8$, $\Delta = 3.0$ and 128^3 resolution model at the different times: $t = 0.5, 1.0, 1.5$ and $2.0 t_{\text{dyn}}$.

6. DISCUSSION

Several authors have already discussed the effects of turbulence (see e.g. Banerjee & Jedamzik 2004; Saveliev et al. 2012; Iapichino & Brüggén 2012; Saveliev et al. 2013; Cho 2014, and many others) and structure formation (see e.g. Dolag et al. 2002; Vazza et al. 2014, and many others) on the evolution of the intergalactic magnetic field. The lack of detection of TeV radiation from blazars points towards the existence of amplified magnetic fields, with filling factors around 60%, even at the intergalactic medium voids (Neronov & Vovk 2010; Dolag et al. 2011). For this reason, turbulence - as a ubiquitous phenomenon - has been preferred as main mechanism for field amplification. The common problem related to turbulent models of collisional plasmas is the typical timescale needed for magnetic field amplification. As explained previously the timescales associated to turbulent amplifications are too large for the magnetic seed amplitudes suggested so far. Structure formation, on the other hand, would be dominant (due to shear, compression or other star-formation related mechanisms) in further amplification of the fields.

In this work we explore a possible scenario for magnetic field amplification at high redshifts (post-recombination), based on the growth of collisionless plasma instabilities. Two similar works have dealt with the problem in a similar approach, being one analytical (Schekochihin & Cowley 2006a) (see also Schekochihin & Cowley 2006b), and the other purely numerical (Santos-Lima et al. 2014). In (Schekochihin & Cowley 2006a) an analytical simplification of the problem is posed, which inspired most of the analytical derivation presented here as well. In their work, however, it is assumed that both, the damping at small scales and the pressure anisotropy Δ , are similarly related to ν_{scat} and ν_{ii} . This in order to obtain the time evolution of Δ and B in terms of an effective collision rate. In the present we do not constrain ν_{scat} which is, in another hand, implicitly constrained to the assumption that Δ is kept constant during the evolution of the system. Interestingly, for the super-exponential phase, both works predict the magnetic field intensity growth rate as $\propto (1 - t/t_c)^{-b}$, though with different slopes and

characteristic timescales. In both estimates the growth of the magnetic field by collisionless instabilities could, in principle, explain the magnetization of the local Universe based on very weak seeds ($< 10^{-17}\text{G}$). Only the analytical model presented in this work has been compared to numerical simulations.

With respect to the numerical solutions, in Kowal et al. (2011) the authors performed simulations with strongly magnetized plasmas and could not address the amplification problem. In this sense, the numerical study presented here stands as an extension of that particular work but focused on the statistical properties of the magnetic field and the role of collisionless plasma instabilities on the amplification of the magnetic field. The scalings found for density and velocity fields in the firehose unstable models of that work resemble those obtained here for the magnetic field, with a power spectrum peak at the smallest scales available in the system. Similar statistical properties were obtained by Santos-Lima et al. (2014), who performed collisionless plasma simulation with variable pressure anisotropy and studied the statistical properties of the magnetic fields as well. The plasma properties were studied in a variable- Δ framework though, with isotropization mechanisms being introduced *ad hoc*. Still, it was shown that even in the cases where isotropization is strong enough to wash out the imprints of instabilities in the statistical properties of the plasma, their dynamical effects are important locally. The amplification of the magnetic field was studied and, as a consequence of small volume coverage of unstable regions, their general conclusion was that the instabilities were not efficient. Differently to the assumption made in this work, their models do not include an external source term to excite the pressure anisotropy, which could - in principle - change the system to a quasi constant- Δ case, similar to ours.

Possible observational evidence (or constraints) for the process described in this work could be obtained from the cosmic microwave background. If collisionality condition was satisfied at pos-equipartition era, the magnetic field at small scales could have been amplified prior to the recombination era, and the ionization structure of the

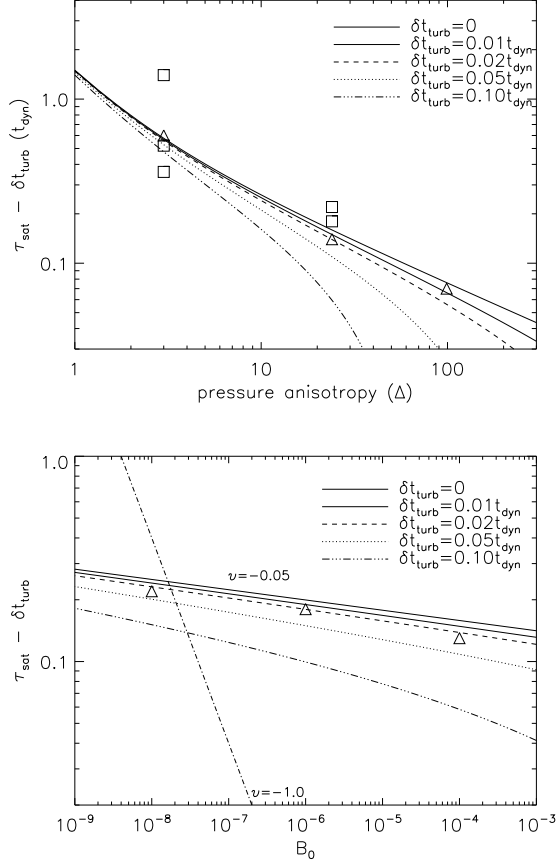


FIG. 8.— Comparison between the numerical simulations and the analytical predictions given in Section 3. *Top*: τ_{gr} vs Δ correlation. Triangles correspond to the simulations with similar initial conditions except for the pressure anisotropy ($\Delta = 3, 24$ and 99), which are the ones used for the correlation analysis. The lines correspond to the solution of Eq.16 for different turbulent delays δt_{turb} (see text). *Bottom*: τ_{gr} vs B_0 correlation. Again, triangle represent the models with similar initial conditions, but now with different seed field intensities ($B_0 = 9 \times 10^8, 9 \times 10^{12}$, and 9×10^{16}). The lines correspond to correlations $\tau_{\text{gr}} \propto B_0^\nu$, being Eq.18 the case with $\nu = -1.0$.

Universe would be different, with effects on Silk damping (see Jedamzik & Abel 2013). On the other hand, if the plasma becomes gyrotropic at $z < z_{\text{rec}}$, such effect would not be relevant.

The main problem with the models mentioned above is the lack of a proper physical description of the isotropization of the particles momenta as the system evolves. Differently to the previous works we consider the balance between pressure anisotropy sources and isotropization effects, which simplifies dramatically the solution of the problem and results in a problem that can be addressed both numerically and analytically. Nature is obviously far more complex than a constant- Δ model, but still any approximated model that can be studied by means of both analytical and numerical methods may be extremely useful to the understanding of the basic dynamical properties related to the dynamics of collisionless plasma fluids.

6.1. Magnetic field characteristic lengthscales

Even if the amplification of the magnetic field, from seed fields up to equipartition levels, could be ex-

plained by the collisionless plasma instabilities, one must still consider its characteristic lengthscale. The zero-dimensional analytical models cannot account for this properly. Still, it is reasonable to consider the typical lengthscale to be that of maximum growth rate. Indeed, from the numerical simulations presented in this work, it has been shown that the turbulent flows cannot modify the magnetic field structure in timescales at which the amplification occurs. The spectral distribution of the magnetic field obtained from the simulations peak at the smallest scales possible, those at which the numerical dissipation overtakes the field growth. The finer the resolution the smaller is the characteristic lengthscale.

In the intergalactic medium this would be given by the natural process that can overtake the pressure anisotropy instabilities, particle collisions. With a typical mean free path of \sim few kpc, one should expect the magnetic field energy to be concentrated in fluctuations with approximately this lengthscale. However, magnetic field correlation lengths as large as \sim Mpc has been inferred from observations (e.g. Ferreti et al. 2012), posing the challenge not only on how to amplify the magnetic field but also on how to distribute the energy from the small to the large scales. In our firehose unstable CGL-MHD models, we obtained power spectra which are steeper than the expected for the kinetic phase of the small-scale dynamo. This demonstrates that the instabilities are indeed the dominant process in place in these models. On the other hand, depending on the level of pressure anisotropy it also results in weaker large scale fields, if compared to the SSD estimates. Given that most of the energy of the magnetic fluctuations are placed at the smallest scale in the gyrotropic fluid approximation (i.e. λ_{mfp}), one could estimate (see Section 3) the magnetic field intensity at large scales as $B_L \sim (|\Delta| p_\perp)^{1/2} (\lambda_{\text{mfp}} L^{-1})$. For $n \simeq 10^{-3} \text{cm}^{-3}$, $kT \simeq 1 \text{eV}$, one finds $B_{\text{Mpc}} \sim \sqrt{\Delta} 10^{-10} \text{G}$.

The answer to this problem may be standing in the properties of the turbulence itself. As discussed earlier in this paper, turbulence stretches and folds the magnetic field in a process that drives the turbulent dynamo. This process is dominant at small scales, and is quenched in a given scale when the magnetic energy reaches equipartition with the turbulent one. In the collisionless plasma the instabilities are responsible for the growth of magnetic field at the small scales. Even though turbulence cannot stretch the field lines at the smallest scales it could, in principle, do it at the largest ones depending on its strength. This is clearly shown in Figs.4, 5 and 6, where the evolution of the turbulent Alfvénic Mach number is always larger than unity, even after the saturation of the magnetic field. This because the velocity dispersion is dominated by the large scale eddies, where equipartition was not reached. For these particular models, the turbulence is responsible for transferring the magnetic field energy from small to large scales. This process should be even more important if the pressure anisotropy is quenched (this is not the case of the simulations, in which we have kept it constant). The quenching of the pressure anisotropy, followed by the transfer of magnetic energy from small to large scales by super-Alfvénic turbulence could therefore explain the observations. In other words, as shown in the numerical simulations, the CGL-MHD instabilities are presumably domi-

nant over the kinematic phase of the small-scale dynamo, but possibly not for the later nonlinear phase (once the instabilities are quenched).

Another possible solution for this problem would be related to the formation of large structures of matter (e.g. massive galaxies, groups and clusters). It is quite clear now that the large scale magnetic field is not primordial, but has constantly evolved with the dynamical evolution of Universe (Jedamzik & Sigl 2011). This was also pointed by Schlickeiser (2005, cf. references therein), in the context of small-scale fluctuations of Weibel instability. The collapse of gas into galaxies or clusters (Vazza et al. 2014), as well as large-scale shears, could in principle amplify coherent components of the magnetic field. If correct, in such scenario magnetic energy would have been provided dominantly at small scales, in the post-recombination era, but reassembled into large scale coherent structures ($> 100\text{kpc}$) following the recent structure formation of the dark and baryonic matter ($z < 10$).

7. SUMMARY

In this work we studied the magnetic field amplification process in turbulent collisionless plasmas. In such plasmas, parallel and perpendicular pressures (with respect to the local magnetic field) may become so anisotropic that instabilities may become dynamically important. It has been pointed in previous analytical models that such instabilities, acting together with a turbulent background, may accelerate the amplification of the magnetic field up to near equipartition levels. Such models would then have dramatic implications on our understanding of the magnetization of the early Universe (post-recombination), given that the intergalactic medium then becomes collisionless. These models provide timescales and saturation estimates for the magnetic energy density, but have never been confronted by full three-dimensional numerical simulations. The aims of this work were to revisit the analytical zero-dimensional models of the magnetic field evolution in turbulent collisionless plasmas and to provide a number of full three-dimensional numerical simulations that could be directly compared to these analytical estimates.

As long as pressure anisotropy is kept constant during the evolution of the system a novel analytical solution is provided for the magnetic field evolution in systems subject to firehose instability. As discussed before, such assumption is not too far from reality, given that different processes act together to increase and decrease pressure anisotropy, and some sort of equilibrium value for Δ , in unstable regime, may exist (specially for weakly magnetized plasmas). We find that:

- for very weak initial seed fields, the early evolution of the magnetic field is dominated by collisions, and the turbulent dynamo should be responsible for the initial amplification of the field;
- once the field grows and $\Omega_i > \nu_{ii}$, a transition from an isotropic to a gyrotropic plasma occurs and instabilities would then be driven. A fraction of the “free-energy” available ($|\Delta|p$) would then be transferred to the magnetic field as the system evolves, up to saturation;
- saturation occurs at $\beta \sim 2/|\Delta|$ value, which is reached in a timescale $\tau_{\text{gr}} \propto B_0^{-1}|\Delta|^\psi$, with $\psi = 1/2$ or $3/2$, for $|\Delta| \gg 1$ and $\ll 1$, respectively.

This analytical model was then compared to a number of CGL-MHD numerical simulations, with different initial and turbulent conditions, from which the evolution of the magnetic field from the seed field, up to saturation, was followed. The main results obtained are as follows:

- the explosive growth of magnetic field energy density is observed in the firehose unstable models, being the amplification timescales approximately proportional to $|\Delta|^\psi$, as was predicted in the simple analytical model;
- there is no clear dependency between τ_{gr} and B_0 in the simulations, in contradiction to the linear anti-correlation derived in the analytical model. This is explained in terms of B_0 being the field intensity at $\Omega \sim \nu_{ii}$ transition, rather than the initial seed value. Also, because the code is unable of evolving the Larmor frequency as a function of B ;
- the power spectrum of the magnetic field peaks at the smallest scales not dominated by the numerical diffusion, and the transfer of energy to large scales must occur afterwards, by turbulence itself, once saturation occurs.

The authors would like to acknowledge the anonymous referee for the useful comments and suggestions that helped improving the current manuscript. We are also very thankful to Alex Schekochihin for valuable discussions about the content of this paper. DFG thanks the European Research Council (ADG-2011 ECOGAL), and Brazilian agencies CNPq (no. 302949/2014-3), CAPES (3400-13-1) and FAPESP (no.2013/10559-5) for financial support. GK acknowledges support from FAPESP (grants no. 2013/04073-2 and 2013/18815-0).

REFERENCES

- Alvelius, K. 1999, *Physics of Fluids*, 11, 1880
 Bale, S. D., Kasper, J. C., Howes, G. G., et al. 2009, *Physical Review Letters*, 103, 211101
 Banerjee, R., & Jedamzik, K. 2004, *Phys. Rev. D*, 70, 123003
 Batchelor, G. K. 1950, *Royal Society of London Proceedings Series A*, 201, 405
 Biermann, L. 1950, *Z. Naturf. A*, 5, 65
 Bonafede, A., Feretti, L., Murgia, M., Govoni, F., Giovannini, G., Dallacasa, D., Dolag, K., & Taylor, G. B. 2010, *A&A*, 513, A30
 Brandenburg, A., Sokoloff, D., & Subramanian, K. 2012, *Space Sci. Rev.*, 169, 123
 Burkhart, B., Falceta-Gonçalves, D., Kowal, G., & Lazarian, A. 2009, *ApJ*, 693, 250
 Chew, G. F., Goldberger, M. L., & Low, F. E. 1956, *Royal Society of London Proceedings Series A*, 236, 112
 Cho, J. 2014, *ApJ*, 797, 133
 de Gouveia Dal Pino, E. M., Santos-Lima, R., Kowal, G., & Falceta-Gonçalves, D. 2013, *IAU Symposium*, 294, 337
 Dolag, K., Bartelmann, M., & Lesch, H. 2002, *A&A*, 387, 383
 Dolag, K., Kachelriess, M., Ostapchenko, S., & Tomàs, R. 2011, *ApJ*, 727, L4
 Donnert, J., Dolag, K., Lesch, H., & Müller, E. 2009, *MNRAS*, 392, 1008

- Dubois, Y., Devriendt, J., Slyz, A., & Silk, J. 2009, *MNRAS*, 399, L49
- Durrer, R., & Neronov, A. 2013, *A&A Rev.*, 21, 62
- Durrive, J.-B., & Langer, M. 2014, *SF2A-2014: Proceedings of the Annual meeting of the French Society of Astronomy and Astrophysics*, 321
- Einfeldt, B. 1988, *SIAM Journal on Numerical Analysis*, 25, 294–318
- Enßlin, T., Vogt, C., & Pfrommer, C. 2005, *The Magnetized Plasma in Galaxy Evolution*, 231
- Falceta-Gonçalves, D., de Gouveia Dal Pino, E. M., Gallagher, J. S., & Lazarian, A. 2010, *ApJ*, 708, L57
- Falceta-Gonçalves, D., Kowal, G., Falgarone, E., & Chian, A. C.-L. 2014, *Nonlinear Processes in Geophysics*, 21, 587
- Federrath, C., Schober, J., Bovino, S., & Schleicher, D. R. G. 2014, *ApJ*, 797, L19
- Feretti, L., Giovannini, G., Govoni, F., & Murgia, M. 2012, *A&A Rev.*, 20, 54
- Gary, S. P., Li, H., O’Rourke, S., & Winske, D. 1998, *J. Geophys. Res.*, 103, 14567
- Gottlieb, S., Ketcheson, D. I. and Shu, C.-W.: High Order Strong Stability Preserving Time Discretizations, *J. Sci. Comp.*, 38, 251–289, 2009.
- Govoni, F., & Feretti, L. 2004, *International Journal of Modern Physics D*, 13, 1549
- Hau, L.-N., & Wang, B.-J. 2007, *Nonlinear Processes in Geophysics*, 14, 557
- Iapichino, L., & Brüggén, M. 2012, *MNRAS*, 423, 2781
- Jedamzik, K., Katalinić, V., & Olinto, A. V. 1998, *Phys. Rev. D*, 57, 3264
- K. Jedamzik and G. Sigl, *Phys. Rev. D* 83, 103005.
- Jedamzik, K., & Abel, T. 2013, *J. Cosm. Astropart. Phys.*, 10, 050
- Kazantsev A.P 1967, *Zh. Eksp. Teor. Fiz.*, 53, 1806. [Transl. 1968 *Sov. Phys. JETP* 26, 10311034.]
- Kim, K.-T., Kronberg, P. P., Giovannini, G., & Venturi, T. 1989, *Nature*, 341, 720
- Kowal, G., Falceta-Gonçalves, D. A., and Lazarian, A., 2011, *New Journal of Physics*, 2011, 13, 053001
- Kraichnan, R. H. 1968, *Physics of Fluids*, 11, 945
- Kronberg, P. P. 1994, *Reports on Progress in Physics*, 57, 325
- Kulsrud, R. M. 1983, *Basic Plasma Physics: Selected Chapters, Handbook of Plasma Physics, Volume 1*, 1
- Kunz, M. W., Schekochihin, A. A., & Stone, J. M. 2014, *Physical Review Letters*, 112, 205003
- Langer, M., Aghanim, N., & Puget, J.-L. 2005, *A&A*, 443, 367
- Mogavero, F., & Schekochihin, A. A. 2014, *MNRAS*, 440, 3226
- Neronov, A., & Vovk, I. 2010, *Science*, 328, 73
- Nikiel-Wroczyński, B., Soida, M., Urbanik, M., Beck, R., & Bomans, D. J. 2013, *MNRAS*, 435, 149
- Planck Collaboration XVI, 2014, *A&A*, 571, A16
- Saveliev, A., Jedamzik, K., & Sigl, G. 2012, *Phys. Rev. D*, 86, 103010
- Saveliev, A., Jedamzik, K., & Sigl, G. 2013, *Phys. Rev. D*, 87, 123001
- Santos-Lima, R., de Gouveia Dal Pino, E. M., Kowal, G., et al. 2014, *ApJ*, 781, 84
- Schekochihin, A. A., Cowley, S. C., Kulsrud, R. M., Hammett, G. W., & Sharma, P. 2005, *ApJ*, 629, 139
- Schekochihin, A. A., & Cowley, S. C. 2006a, *Physics of Plasmas*, 13, 056501
- Schekochihin, A. A., & Cowley, S. C. 2006b, *Astronomische Nachrichten*, 327, 599
- Schekochihin, A. A., Iskakov, A. B., Cowley, S. C., et al. 2007, *New Journal of Physics*, 9, 300
- Schlickeiser, R., & Shukla, P. K. 2003, *ApJ*, 599, L57
- Schlickeiser, R. 2005, *Plasma Physics and Controlled Fusion*, 47, A205
- Schober, J., Schleicher, D., Federrath, C., Klessen, R., & Banerjee, R. 2012, *Phys. Rev. E*, 85, 026303
- Schober, J., Schleicher, D. R. G., & Klessen, R. S. 2013, *A&A*, 560, A87
- Soucek, J., Lucek, E., & Dandouras, I. 2008, *Journal of Geophysical Research (Space Physics)*, 113, A04203
- Tóth, G.: The $\nabla \cdot \mathbf{B} = 0$ Constraint in Shock-Capturing Magnetohydrodynamics Codes, *J. Chem. Phys.*, 161, 605–652, 2000.
- Trivedi, P., Subramanian, K., & Seshadri, T. R. 2010, *Phys. Rev. D*, 82, 123006
- Xu, H., Li, H., Collins, D. C., Li, S., & Norman, M. L. 2009, *ApJ*, 698, L14
- Xu, H., Govoni, F., Murgia, M., et al. 2012, *ApJ*, 759, 40
- Vacca, V., Murgia, M., Govoni, F., Feretti, L., Giovannini, G., Perley, R. A., & Taylor, G. B. 2012, *A&A*, 540, A38
- van Leer, B. 1974, *J. Chem. Phys.*, 14, 361
- Vazza, F., Brüggén, M., Gheller, C., & Wang, P. 2014, *MNRAS*, 445, 3706
- Widrow J. M. 2002, *RevModPhys*, 74, 775
- Widrow, L. M., Ryu, D., Schleicher, D. R. G., et al. 2012, *Space Sci. Rev.*, 166, 37
- Winterhalter, D., Neugebauer, M., Goldstein, B. E., et al. 1995, *Space Sci. Rev.*, 72, 201